Synthesis and Evaluation of Cationic Porphyrin-based Organic Nanocages for the Removal of 38 PFAS from Water: Experimental, Theoretical, and Eco-Toxicological Insights

Karla R. Sanchez-Lievanos[1]*; Daoyang Zhang[2]; Scott M. Simpson[3]; Mindula K. Wijayahena[2]; Gina Rizzo[4]; John Michael N. Aguilar[2]; Liezel Mari Abaya[2]; Julia M. Dovi[4]; Howard I. Sirotkin[4]; Matthew R. Crawley[2]; Timothy R. Cook*[2]; Diana S. Aga*[1,2]

[1]University at Buffalo Research and Education in Energy, Environment and Water (RENEW) Institute, The State University of New York, Buffalo, New York 14260, United States.
[2]Department of Chemistry, University at Buffalo, The State University of New York, Buffalo, New York 14260, United States.
[3]Department of Chemistry, St. Bonaventure University, St. Bonaventure, New York 14778, United States.
[4]Department of Neurobiology and Behavior, Stony Brook University, Stony Brook, New York 11794, United States.

Abstract

Per- and polyfluoroalkyl substances (PFAS), persistent pollutants found in water sources worldwide, pose significant challenges to conventional remediation methods. This study presents a one-pot, high atom-economy synthesis of porphyrin-based cationic nanocages (oNCs) as a selective, rapid and efficient solution for PFAS removal, addressing critical gaps in current water treatment technologies. Using liquid chromatography-tandem mass spectrometry (LC-MS/MS), the nanocages—**[oNC]8PF$_6$**, **[Co^{2+}-oNC]8PF$_6$**, and **[Co^{3+}(N≡O)-oNC]8PF$_6$**—were evaluated for their ability to sorb a mixture of 38 PFAS, including emerging contaminants like GenX, from various water matrices at a concentration of 50 ng/mL. The nanocages achieved exceptional PFAS removal efficiencies, with optimal results obtained when **[oNC]8PF$_6$** and **[Co^{2+}-oNC]8PF$_6$** were combined in a 1:4 ratio. This mixture created a synergistic effect, enabling the sorption of both short- and long-chain PFAS, achieving average removal efficiencies of 90% in Nanopure^{TM} and groundwater, and 80% in influent sewage. The nanocage mixture consistently outperformed activated carbon, particularly in complex matrices such as influent sewage, where activated carbon presented lower efficiency, especially for perfluoroalkane sulfonamido substances. The nanocages reached sorption equilibrium within 15 minutes and maintained performance across multiple methanolic regeneration cycles, highlighting their operational durability. NMR spectroscopy and computational studies revealed that PFAS sorption occurs *via* hydrophobic and electrostatic interactions, as well as partial intercalation, with selectivity for PFAS molecules bearing sulfonate and sulfonamide head groups and carbon chain lengths of five or more. Early-stage eco-toxicological assessments confirmed the environmentally safety of these nanocages, showing no adverse effects below a concentration of 0.005 μM. By combining rapid PFAS removal with modular, scalable and sustainable material synthesis, this study sets a new direction for developing precise, environmentally responsible PFAS water treatment solutions.

Keywords: Per- and polyfluoroalkyl substances (PFAS); cationic porphyrin-based nanocages; efficient removal; selectivity, nanotoxicity.

Synopsis

Porphyrin-based nanocages are safe, selective, and highly effective materials for removing "forever chemicals" from water, providing a solution for cleaner, safer water.

1. Introduction

Per- and polyfluoroalkyl substances (PFAS) are a class of synthetic organic compounds that have raised significant environmental and health concerns due to their widespread presence and persistence in the environment. Addressing PFAS contamination in water is a critical global challenge, as existing remediation technologies, such as activated carbon, ion exchange resins, and reverse osmosis, often have weak interactions with PFAS or require costly maintenance/installation, and typically involve energy-intensive regeneration processes.[1, 2] Consequently, there is a growing interest in developing advanced materials for more efficient and cost-effective PFAS remediation.[3] Recently, inorganic and organic nanoporous materials, such as metal-organic frameworks (MOFs),[4, 5] zeolitic imidazolate frameworks (ZIFs),[6] covalent organic frameworks (COFs),[7, 8] hydrogen-bonded organic frameworks (HOFs),[9, 10] and molecular nanocages,[11-13] have emerged as promising candidates for pollutant removal from water. Their robust and customizable structures have demonstrated remarkable removal capacities to capture and chemically deactivate hazardous substances, effectively encapsulating, adsorbing, or even degrading various noxious gases, toxic organophosphorus compounds, water pollutant oxyanions, and emerging organic contaminants.[11, 14-17] These materials can be designed to incorporate specific functional groups, pore sizes, and shapes, thereby enabling tailored interactions with target molecules. A critical advantage of molecular nanocages, such as porphyrin-based nanocages, lies in the fact that these molecular building blocks can be pre-designed with specific functionalities to incorporate highly sorption-active sites. This contrasts with MOFs, COFs, and other porous materials where the active sites are typically part of the larger framework's structure, often requiring post-synthetic modifications to enhance functionality.[18, 19] Therefore, the synthetic precision and chemical selective available for molecular nanocages offers an exquisite avenue for next-generation environmental remediation materials.[20]

Porphyrins and their molecular nanocage analogs have emerged as versatile compounds with diverse applications in environmental science, including the removal of dyes, hormones, antibiotics, insecticides and phenolic xenoestrogens in water.[21, 22,22-29] The synthetic opportunity to extensively modify these molecular nanocages through adjustments of central metal ions and functional groups, and their capability to achieve pollutant sorption-desorption equilibrium within minutes—an efficacy that surpasses the performance of conventional materials,[15, 16] make these materials suitable as sorbents for emerging pollutants, such as PFAS. For instance, in 2022, Zhu *et al.* reported the successful application of a porphyrin-based two-dimensional layered MOF to degrade organic dyes and inactivate bacteria by generating reactive oxygen species (ROS), under

light and ultrasound.[28] Sun *et al.* also reported the use of a Cobalt-based porphyrin complexes to reductively defluorinate up to 51% branched perfluorooctanesulfonic acid (PFOS) under mild conditions.[27] Moreover, Zhang *et al.* observed high adsorption capacity, fast kinetics, and strong selectivity of a porphyrinic MOF towards PFOS, PFHxS, and PFBS, even in the presence of competing anions and humic acid.[29] However, these studies focus on a limited range of PFAS, leaving their effectiveness against a broader spectrum of PFAS or in real-world water matrices uncertain. Furthermore, material scalability remains unclear due to complex, multi-step synthesis and challenges in maintaining consistent material quality.

The objectives of this study are: (*i*) to present a one-pot synthesis method for porphyrin-based nanocages that simplifies the traditionally multi-step purification process, improves atom economy, and increases reaction yield, while also reducing production costs by utilizing commercially available reagents; (*ii*) to address a critical research gap by enhancing the removal efficiency of short-chain PFAS, specifically testing the nanocages' performance across a mixture of 38 PFAS in nanopure^{TM}, ground, and influent sewage water, and (*iii*) to conduct early-stage ecotoxicity assessments of the synthesized nanocages to evaluate their potential environmental impact and guide future modifications for improved safety and efficacy. We use a library of porphyrin-based agents including (*i*) a metal-free organic nanocage (**[oNC]8PF$_6$**), and two metal-organic nanocages, (*ii*) **[Co^{2+}-oNC]8PF$_6$** and (*iii*) **[Co^{3+}(N≡O)-oNC]8PF$_6$** (Scheme 1). We selected these architectures for their robustness in aqueous environments, hypothesizing that their cationic and hydrophobic properties, coupled with accessible internal cavities, could provide the basis for interactions with broad classes of PFAS, and facilitate easy recovery and reuse after PFAS sorption. We evaluated the performance of the three cages in 50 ng/mL aqueous solutions containing 38 of the 40 PFAS listed in the EPA Draft Method 1633, including GenX, which is more toxic and mobile than the chemical they were developed to replace: PFOA.[30, 31] Additionally, we explored the interactions between PFOS and **[oNC]$^{8+}$**, employing both NMR spectroscopy and computational modeling to visualize the sorption sites of this nanocage. There are several novel aspects of this study: First, we carried out combinatorial experiments to optimize mixtures of two porphyrin-based nanocages, **[oNC]8PF$_6$** and **[Co^{2+}-oNC]8PF$_6$**, which, to our knowledge, is the first approach leveraging synergy in molecular interactions to achieve significant removal of both long-chain and short-chain PFAS. Second, we established that the structural integrity of these nanocages is maintained across a wide pH range and over multiple sorption cycles, a critical factor for their durability in practical applications. Finally, we benchmarked our optimized mixture against activated carbon (CAS No. 7440-44-0) in both influent sewage water and groundwater, showcasing its superior performance in real-world conditions. Additionally, recognizing the limited studies on the long-term impacts of nanoscale materials, this study is the first to evaluate the ecotoxicity of **[oNC]8PF$_6$** and **[Co^{2+}-oNC]8PF$_6$** through behavioral assays in zebrafish embryos. This comprehensive approach not only emphasizes the ecological safety of these materials but also highlights their potential for sustainable and effective environmental remediation.

Scheme 1. Cationic oNCs containing a cofacial porphyrin motif used as PFAS sorbents.

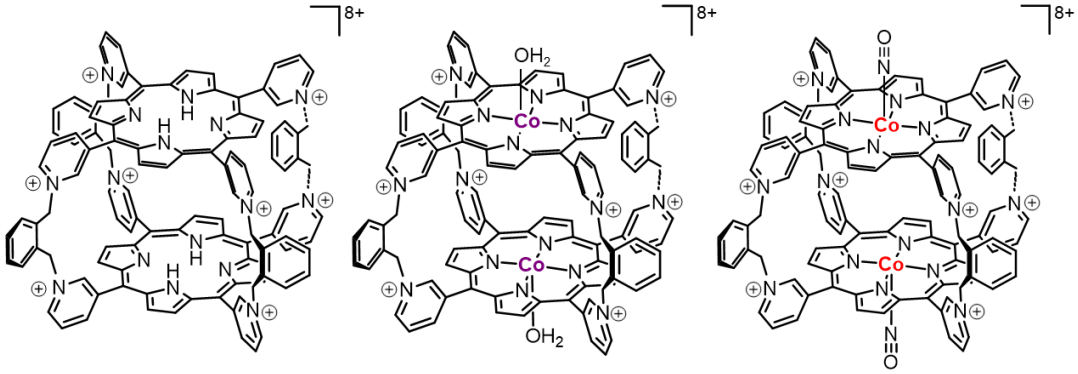

2. Materials and Methods

*2.1. Synthesis of nanocages **[oNC]8PF6***: **[oNC]8PF6** was prepared using a recently developed method established by Zhang *et al*.[32] 1,2-Dibromoxylene (2.6 g, 10 mmol) was added to a solution of 5,10,15,20-tetra(pyridin-3-yl)porphyrin (T3PyP) (309.3 mg, 0.5 mmol) in DMF (100 mL). After heating at 120°C for 24 hours, the mixture was cooled and concentrated to ~50 mL. It was then added to CH_2Cl_2, and the precipitate was filtered and washed with CH_2Cl_2 (3 × 50 mL). The dark brown solid was dissolved in H2O, filtered, and NH_4PF_6 was added to the filtrate to precipitate the solid. The solid was filtered, washed with water (3 × 50 mL), dried overnight, and collected as a dark red solid (Yield: 643 mg, 91.5%). ^{1}H NMR (500 MHz, CD_3CN) δ 9.47 (d, 8H pyridyl), 9.00 (d, 8H pyridyl), 8.85 (s, 8H pyridyl), 8.48 – 8.68 (m, 24H pyrrolic, pyridyl), 7.79 (dd, 8H xylene phenyl), 7.47 (dd, 8H xylene phenyl), 6.33 (s, 16H xylene methylene), -4.40 (s, 4H pyrrolic NH). ESI-MS: m/z = 1261.747, $[oNC + 6PF_6^-]^{2+}$, m/z = 792.833, $[oNC + 5PF_6^-]^{3+}$ m/z = 558.452, $[oNC + 4PF_6^-]^{4+}$

*2.2. Synthesis of nanocage **[Co2+-oNC]8PF6***: **[Co2+-oNC]8PF6** was prepared by a modified literature procedure.[33] A solution of **[oNC]8PF6** (90 mg, 0.032 mmol) in acetonitrile (~10 mL) was stirred, and $Co(OAc)_2 \cdot 4H_2O$ (64 mg, 0.32 mmol) in acetonitrile (~10 mL) was added. The mixture was refluxed for 18 hours, then cooled and concentrated to ~10 mL. The mixture was added dropwise to an NH_4PF_6 solution (0.5 g in 50 mL water), forming a red precipitate. The precipitate was filtered, washed with water (3 × 20 mL), dried overnight, and collected as a dark red solid (Yield: 87 mg, 92.8%). ^{1}H NMR (500 MHz, CD_3CN) δ 11.5 (s, 16H pyrrolic), 9.69 (s, 16H pyridyl), 9.12 (s, 16H pyridyl), 8.16 (dd, 8H xylene phenyl), 7.9 (dd, 8H xylene phenyl), 6.66 (s, 16H xylene methylene). ESI-MS: m/z = 1318.705, $[oNC + 6PF_6^-]^{2+}$, m/z = 830.785, $[oNC + 5PF_6^-]^{3+}$ m/z = 586.847, $[oNC + 4PF_6^-]^{4+}$ m/z = 440.488, $[oNC + 3PF_6^-]^{5+}$.

*2.3. Synthesis of nanocage **[Co3+(N≡O)-oNC]8PF6***: Nitric oxide gas was generated as per a literature procedure.[34] **[Co3+(N≡O)-oNC]8PF6** was prepared using a modified Lipke *et al.* method.[34] **[Co2+-oNC]8PF6** (58 mg, 0.02 mmol) was dissolved in 5 mL acetonitrile in a sealed Schlenk flask and bubbled with nitric oxide for 10 mins, changing color from dark red to slightly orange. The solution was added to 10 mL DCM, precipitating a red solid. This solid was collected

by centrifugation and dried under vacuum, yielding **[Co^{3+}(N≡O)-oNC]8PF_6** as a red solid (32.5 mg, 55.9%). ^{1}H NMR (500 MHz, CD_3CN) δ 9.41 (d, 8H pyridyl), 9.26 (d, 8H pyridyl), 8.67 (s, 8H pyridyl), 8.58 – 8.62 (m, 24H pyrrolic, pyridyl), 7.68 (dd, 8H xylene phenyl), 7.20 (dd, 8H xylene phenyl), 6.16 (s, 16H xylene methylene).

2.4. Optimal Nanocage Load and Equilibration Time for PFAS Removal: To determine the optimal nanocage mass and equilibration time for PFAS capture, we tested 0.3 to 1.8 mg of nanocage in a 200-µL PFAS solution (50 ng/mL) containing PFCAs with carbon chains of four to nine. Evaluations were done at intervals from 1 to 60 minutes under constant shaking at 200 RPM. Samples were then prepared for LC-MS/MS analysis as detailed below.

2.5. PFAS Removal Experiments and Sample Preparation: Nanopure^{TM} water solutions (200 µL) containing 50 ng/mL of each of the 38 PFAS from EPA Draft Method 1633 (Table S1) were mixed with the nanocage by vortexing and shaken for 15 minutes. Control samples were also monitored. The suspensions were centrifuged at 2,007 g for 15 minutes, and the supernatant was spiked with 25 ng/mL of an isotopically labeled PFAS mixture (MPFAC-24ES, Table S2) from Wellington Laboratories. The supernatant was subsequently mixed with the mobile phase (refer to Liquid Chromatography with Tandem Mass Spectrometry (LC-MS/MS) section) to achieve a final concentration of 25 ng/mL. Then an isotopically labeled standard was spiked into the sample, which was finally vortexed and then analyzed by LC-MS/MS for quantification. All samples were analyzed in triplicate for accuracy and reproducibility.

2.6 Environmental Matrix Effects on oNCs-PFAS Interactions: The effects of environmental matrices on oNCs-PFAS interactions were investigated using triplicate samples of real influent sewage water and groundwater. The samples were first filtered to remove solids. Following the method outlined by Camdzic *et al.,*[16] 500 mL of influent sewage water and groundwater were adjusted to a pH of 2.5 ± 0.5 using glacial acetic acid. The samples were then processed through tandem Oasis HLB and Oasis WAX solid phase extraction (SPE) cartridges, which had been preconditioned with 10 mL of methanol (MeOH) followed by 10 mL of water. Elution was carried out using 5 mL of 0.1% NH4OH in methanol, methanol, and acetonitrile at a flow rate of 3−5 mL/min for each solvent. The combined eluates were concentrated to 500 µL under a gentle stream of nitrogen gas at room temperature. The dried extracts served as matrix samples, which were then spiked to a final concentration of 50 ng/mL. These spiked matrix samples were then exposed to the nanocages as described in the *PFAS Removal Experiments and Sample Preparation* section.

2.7 Liquid Chromatography with tandem mass spectrometry (LC-MS/MS): PFAS quantification was performed using an Agilent 1200 HPLC coupled to a Thermo ScientificTM TSQ Quantum Ultra triple quadrupole mass spectrometer (LC-MS/MS) in negative mode electrospray ionization (-ESI) with a spray voltage of +3000 V and capillary temperature of 300°C. Nitrogen served as the sheath gas (35 arb.) and auxiliary gas (30 arb.). A Restek Raptor C18 column (2.7 µm, 100 x 3 mm) was used with a mobile phase of 5 mM ammonium acetate (A) and methanol (B) at 0.270 mL/min. A 27-minute gradient method started with 55% B, ramped to 95% B over 13 minutes, held for 9 minutes, and returned to 55% B over 0.5 minutes, holding for 5 minutes. For Gen X analysis, an isocratic elution with 40% A and 60% B was used. Both capillary and vaporizer temperatures were set at 100°C, with sheath gas and auxiliary gas pressures at 10 arb. PFAS

quantification used isotopic dilution. See *Supporting Information* for all materials needed for LC-MS/MS.

2.8. Nuclear Magnetic Resonance: ^{1}H and ^{19}F NMR spectra for pre and post treatment were acquired on a Bruker AVANCE NEO 500 (11.75 T, operating at 500 MHz (^{1}H) and 470.4 MHz (^{19}F)) NMR spectrometers (Billerica, MA). Chemical shifts (δ) are reported in parts per million (ppm) relative to the residual proton solvent peaks for ^{1}H NMR. Data were processed using MNova 14.1.2 software version.

2.9. High Resolution Mass Spectrometry: High resolution mass spectra to confirm m/z of **[oNC]8PF$_6$**, **[oNC]8Br**, **[Co^{2+}-oNC]8PF$_6$**, and **[Co^{3+}(N≡O)-oNC]8PF$_6$** were acquired on a Bruker Solarix 12T ESI-FT-ICR (Billerica, MA).

2.10. Single-crystal X-ray Diffraction: Single crystals of **[oNC]8PF$_6$** were grown from a DMF/diethyl ether solution and extracted using N-Paratone oil. The sample was mounted on a MiTeGen loop and analyzed with a Rigaku XtaLAB Synergy-S diffractometer equipped with PhotonJet-S Cu and Ag microfocus sources and a HyPix-6000HE detector. Further information can be found in the *Supporting Information*.

2.11. Scanning Electron Microscopy: SEM micrographs were obtained using a Zeiss Auriga scanning electron microscope with a beam energy of 25 kV. The samples were drop-cast onto silicon wafers from hexane dispersions.

2.12. Computational Calculations: Density functional theory with empirical dispersion correction calculations, specifically DFT-D3(BJ), were carried out to further elucidate the binding affinity and the specific mode of PFAS sorption onto the nanocage. To elucidate the most likely binding site of the PFOS anion in relation to the cage, a series of DFT geometry optimizations with a variety of different functionals were performed. To quantify the strength of this interaction, the binding energy between the cage and the adsorbate was systematically calculated using computational methods described in the methods section of the *Supporting Information*. The binding energy ($\Delta E_{binding}$) of the PFAS molecules was determined using the following formula:

$$\Delta E_{binding} = E_{PFAS-cage} - E_{PFAS} - E_{cage} \qquad (1)$$

where $E_{PFAS\text{-}cage}$ represents the energy of the complex with the PFAS molecule bound inside the cage, E_{PFAS} is the energy of the isolated, optimized PFAS molecule in its anionic form, and E_{cage} denotes the energy of the isolated, optimized cage. A negative $\Delta E_{binding}$ represents an energetically favorable interaction, whereas a positive value indicates an unfavorable one. The binding energy calculations were conducted using four distinct density functionals—BP86-D3(BJ), PBE-D3(BJ), PBE0-D3(BJ), and TPSS-D3(BJ)—each representing a different tier on "Jacob's Ladder" of density functional approximations (See *Supporting Information*).[35]

All structures were initially constructed optimized using the UFF force field in the program Avogadro.[36] All density functional theory (DFT) calculations were conducted using TURBOMOLE,[37, 38] and the def2-TZVP2 basis set[39, 40] from the TURBOMOLE basis set library. DFT calculations were conducted with BP86,[41-43] PBE,[44, 45] PBE0,[43-45] or TPSS[44, 46] functionals.[47,

[48] The Grimme3 dispersion correction with BJ-damping was used to account for dispersion interactions.[49, 50] For all PFAS considered herein, the anionic form was considered during the calculations given their predicted and measured acid dissociation constants.[51-53] The COnductor-like Screening MOdel (COSMO) continuum solvation model with a dielectric constant value of 84.39 for water was utilized in all calculations.[54 52, 53, 55-58]

2.13. Eco-toxicity Assessment: Behavioral assays in zebrafish embryos were employed as a sensitive and insightful ecotoxicity marker, enabling early identification of potential adverse effects from these molecular nanocages. Zebrafish offer several advantages that make them an ideal model for such analyses. They are easily cultured and produce large numbers of rapidly developing transparent embryos that facilitate both morphological and complex behavioral studies in a controlled laboratory environment. [59, 60] Detailed methodologies are provided in the *Supporting Information*.

2.13.1. Zebrafish husbandry: The wild-type fish used is a hybrid strain consisting of Tüpfel long fin and Brian's wild type. The larvae were grown in 24-well polystyrene Falcon tissue culture plate, 1 embryo per well. All experiments and procedures were approved by the Stony Brook University Institutional Animal Care and Use Committee (#269492). All animal work was overseen by the Division of Laboratory Animal Resources (DLAR) at Stony Brook University. DLAR provides veterinary care and assures compliance with local, state, and federal regulations and policies. All information about nanocage treatment, Zebrafish spontaneous and photic-evoked locomotor behavior and Experimental design and statistical analysis, can be found in the *Supporting Information.*

2.13.2. Nanocage treatment: **[oNC]8PF$_6$** and **[Co^{2+}-oNC]8PF$_6$** were suspended in 100 mL of egg water (6 g of synthetic sea salt, 20 ml of methylene blue (1 g/L) solution in 20 L of water, pH 7), to create a 50 mM stock. Treatments consisted of 2.5 μM, 0.5 μM, 0.05 μM, and 0.005 μM. Each well of the 24 well dish was filled with 1.5 mL of the corresponding solution and embryos were placed in the well at 24 hours post fertilization (hpf).

2.13.3. Zebrafish spontaneous and photic-evoked locomotor behavior: Behavioral assays used mixed pools of embryos from multiple parents to minimize genetic effects. At 6 days post-fertilization (dpf), behavior was recorded using a Zebrabox imaging system and Zebralab video-tracking software. The paradigm involved 20 minutes of light acclimation, followed by 15 minutes of light and 15 minutes of darkness. Motor movements were measured by count, duration, and distance. Photic responses were measured by the distance larvae moved in 1 second after the light was extinguished.[61, 62]

2.13.4. Experimental design and statistical analysis: Data analysis was done using R Studio and Excel. Averages are shown as mean ± SEM. Each treatment group had 48 samples from two averaged trials. One-factor ANOVA followed by Tukey's post hoc test determined significance, with $p < 0.05$ as the threshold. Zebrafish sex was not a factor at 6 dpf.

3. Results and Discussion

3.1 Synthesis and characterization of oNCs

Traditional synthetic approaches for synthesizing cofacial porphyrins include multi-step organic tethering approaches that require multiple chromatographic purification steps to obtain milligram quantities, or self-assembly methods that use molecular clips based on precious metals.[63-68] The method used here advances this field by enabling the formation of water-stable, robust molecular nanocages through a straightforward, catalyst-free synthesis under mild conditions. This process requires no column purifications and eliminates the use of metal nodes and/or air-sensitive reactants. Post-synthetic metal insertion into these porphyrin-based nanocages is straightforward, enhancing their structural versatility and reducing overall synthetic efforts. We explored various transition metals and selected cobalt for its ability to form nanocages with higher yield and excellent stability in water, which was tested across a broad pH range (See Figure S2B).

Scheme 2 presents an overview of the oNCs synthesis pathway. **[oNC]8PF$_6$** was synthesized by combining 1,2-dibromoxylene and 5,10,15,20- tetra(pyridine-3-yl)porphyrin (T3PyP) in DMF at 120°C for 24 hours–leading to the formation of **[oNC]8Br**–followed by anion exchange with NH_4PF_6 to yield **[oNC]8PF$_6$** as a dark brown precipitate in water.[32, 33] **[Co^{2+}-oNC]8PF$_6$** was prepared as a red precipitate using a modified previously reported method,[34] involving overnight reflux of **[oNC]8Br** and $Co(OAc)_2{\cdot}4H_2O$ in acetonitrile, and subsequent precipitation with NH_4PF_6. **[Co^{3+}(N≡O)-oNC]8PF$_6$** was synthesized by dissolving **[Co^{2+}-oNC]8PF$_6$** in acetonitrile in a sealed Schlenk flask. The solution was bubbled with nitric oxide for 10 minutes, resulting in the dark red solution becoming slightly more orange. **[Co^{3+}(N≡O)-oNC]8PF$_6$** precipitated as a red powder upon the addition of DCM. All cages were identified by ^{1}H NMR spectroscopy (Figure 1A), ESI-HRMS (Figures 1B and S1), UV-Vis (Figure S2, S11) and SEM (Figure S3). Nanocage **[oNC]8PF$_6$** was characterized by single-crystal X-ray diffraction (SCXRD). Further details of the syntheses, isolations, and characterizations of the molecular cages can be found in the *Supporting Information*.

Scheme 2. Synthesis pathway of the porphyrin-based cationic organic nanocages.

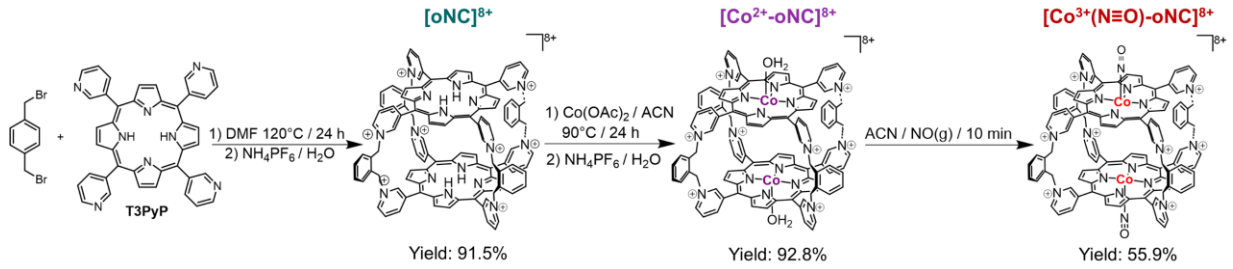

The structures of all cages were confirmed by ^{1}H NMR spectroscopy. **[oNC]8PF$_6$**, **[oNC]8Br**, and **[Co^{3+}(N≡O)-oNC]8PF$_6$** are diamagnetic species and their NMR spectra share three distinct regions: the region from ~10 to 8 ppm encompasses pyridyl and pyrrolic proton

resonances. Between ~8 to 7 ppm, peaks corresponding to the xylene proton resonances are observed. Lastly, the ~7 to 6 ppm interval contains resonances from the CH_2 protons linking the xylene and the pyridinium groups. For **[Co^{2+}-oNC]8PF$_6$**, peaks were broad, indicative the paramagnetic nature of d^7 Co^{2+} centers. The bis-porphyrin architecture and 8+ charge were confirmed by electrospray ionization high resolution mass spectrometry (ESI-HRMS). The mass spectrum of **[oNC]8PF$_6$** and **[Co^{2+}-oNC]8PF$_6$**, are shown as an example of the data obtained (Figure 1B). For all cages, the parent ion peak was either a 3+ or 4+ peak, corresponding to unfragmented cores balanced by five and four PF_6 counterions, respectively. The m/z values and charge states collectively support our structural assignment and that the cages persist in solution.

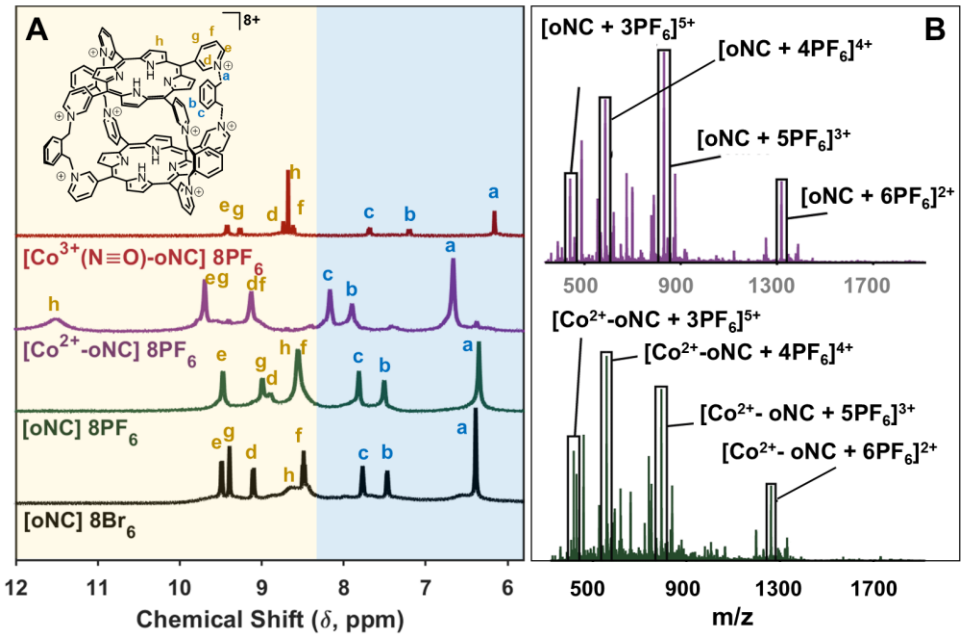

Figure 1. (**A**) ^{1}H NMR of all cages in d_3-acetonitrile (PF_6 salts), and in d_2-water for (Br salts), recorded at 500 MHz. Porphyrin peaks (yellow panel): 8.5 – 12.0 ppm (f, h, d, g, e); xylene peaks (blue panel): 6.0 – 8.0 ppm (a, b, c). (**B**) High resolution mass spectrum of **[oNC]8PF$_6$** (*bottom*) and **[Co^{2+}-oNC]8PF$_6$** (*top*) acquired in acetonitrile. Labelled peaks correspond to the intact cores ionized by loss of PF_6^- counter ions.

Crystals suitable for SCXRD analysis were obtained by vapor-diffusion of diethyl ether into a DMF solution of **[oNC]8PF$_6$**. The structure of **[oNC]8PF$_6$** (Fig. 2A) has a coplanar arrangement of its porphyrin faces with a centroid-to-centroid separation of 7.1 Å. The xylene spacers fold inward imparting a quasi-C_4 rotation axis to the structure. When viewed down this axis, the distances between opposite benzylic carbons, which represent the largest spans across the structure, are 15.3 Å and 16.0 Å, illustrated in Figure 2 as L1 and L2, respectively. Additionally, the folding over of the xylene groups creates pockets occupied by PF_6^- anions, shown in Figure S4, which may act as external recognition sites when the anions are displaced by analytes of interest. In addition to being a structural cavity, the nearby cationic pyridinium moieties enhance

electrostatic interactions at these positions. Furthermore, the internal cavity of the structure is capable of accommodating guests with a volume comparable to four DMF molecules, as shown in Figure S4. The possibility of multiple non-covalent interactions within these structures raises questions about the encapsulation mechanism and the capacity to adsorb specific PFAS molecules, which are addressed in section 3.6.

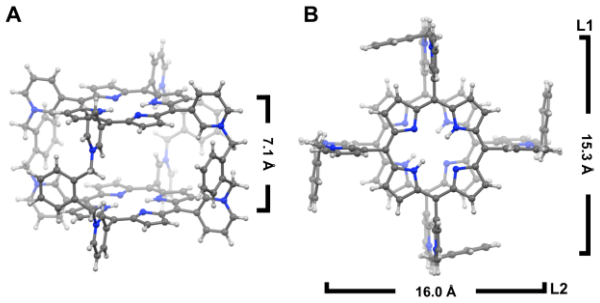

Figure 2. Crystal structure of **[oNC]8PF$_6$**. (**A**) Lateral view. Atom (color): N (blue); C (gray); H (white). (**B**) Top view showcasing the arrangement and distortions of the xylene spacers.

3.2 Nanocages as sorbents for PFAS

3.2.1 Selective adsorption analysis of structurally categorized PFAS

The affinity of nanocages **[oNC]8PF$_6$** and **[Co^{2+}-oNC]8PF$_6$** towards a spectrum of PFAS was comprehensively evaluated in Nanopure^{TM} water. The experimental framework was constructed around a diverse set of PFAS, categorized into three distinct groups, namely carboxylic acids (PFCAs), sulfonic acids (PFSAs), or ether derivatives (PFECAs and PFESAs). Within these groups, we included variations in chain lengths from four to nine carbons, as shown in Scheme S1. These experiments were designed to reveal the relationship between the head groups and overall size on removal efficiencies of PFAS by **[oNC]8PF$_6$** and **[Co^{2+}-oNC]8PF$_6$**. We evaluated various equilibration times and oNC dosages, detailed in Figure S5. We selected 50 ng/mL for all our PFAS studies. Although this concentration is not environmentally relevant, it was selected because it allowed us to measure remaining PFAS in solution without pre-concentration based on the current limits of detection (LOD) of our LC-MS/MS instrumentation. The detection of removal efficiency spans an average percentage range from approximately 3.8% to 100% of the original PFAS concentration (Table S3). At this concentration, our analytical methods can reliably and accurately detect and quantify PFAS, ensuring robust and reproducible data. Ultimately, our results indicated that using 9 mg/mL of cage to treat 50 ng/mL solution of PFAS required only a 15-minute equilibration period for percentage removals of over 80% of these pollutants from aqueous samples. Given the removal efficiencies observed, it was unnecessary to investigate loadings beyond 9 mg/mL, as further increases are unlikely to yield additional benefits.[69, 70] The empirical data, illustrated in Figure S6, showed that both nanocages exhibited a strong affinity for PFAS from all three groups with carbon chains longer than five carbons. In addition, nanocage **[Co^{2+}-oNC]8PF$_6$** demonstrated superior performance over **[oNC]8PF$_6$**, as evidenced by its capacity to remove at least 5% more shorter-chain PFAS from all three categories (Table 1). This difference

in performance is further demonstrated by the improved adsorption of individual short-chain PFAS when comparing non-metalated to metalated oNC PFAS-treated scenarios, as shown in Figure S5C. The enhanced adsorption of short-chain PFAS after metalation is likely due to specific interactions between the cobalt center and PFAS molecules, involving coordination chemistry and hydrogen bonding.[71-74] These interactions are especially important for short-chain PFAS, which rely more on electrostatic forces for adsorption due to their weaker van der Waals interactions. This prompted us to explore a higher oxidation state of the metal center in the nanocage system, transitioning from **[Co^{2+}-oNC]8PF_6** to **[Co^{3+}(N≡O)-oNC]8PF_6**. The enhanced cationic nature of this system was hypothesized to improve not only overall removal efficiency but also selectivity across a wider array of PFAS compounds, particularly to ascertain selectivity concerning chemical head groups.

3.2.2 Mixture effects on the removal of 38 PFAS

We subjected all three nanocage variants (**[oNC]8PF_6**, **[Co^{2+}-oNC]8PF_6** and **[Co^{3+}(N≡O)-oNC]8PF_6** to a mixture of 38 distinct PFAS compounds, including GenX, in Nanopure™ water at a neutral pH (see *Supporting Information* for PFAS-specific graphs, Figure S7). We observed enhancement in PFAS removal efficiencies in the order of **[oNC]8PF_6** < **[Co^{2+}-oNC]8PF_6** < **[Co^{3+}(N≡O)-oNC]8PF_6**. The presence of a metal center in the architecture appears to play a key role in the favorable removal of short-chain PFAS, with an increased removal efficiency, as we transitioned from using **[oNC]8PF_6** to **[Co^{3+}(N≡O)-oNC]8PF_6**, from 67 ± 3% to 84 ± 1% for PFBA, 70 ± 5% to 89 ± 2% for PFMPA and 90 ± 4% to 98 ± 2% for GenX (see Table 1). The increased removal of short-chain PFAS by the nanocages is likely due to metalation and higher oxidation states, which enhance electrostatic interactions and metal complexation. This behavior may result from axial coordination of PFAS carboxylic headgroups with the metal centers, as supported by studies on metal-loaded chitosan and nanocellulose-metal oxide composites (Figure 3, Table S4).[73, 75-77] Moreover, we observed that, in general, sulfonate and alkane sulfonamido PFAS (PFSAs and PASAs, respectively) had higher removal efficiencies, highlighting the affinity of the nanocages towards PFAS with higher electron density headgroups. This observation highlights the role of chemical modification in improving the selectivity of nanocages towards a broad spectrum of PFAS contaminants.

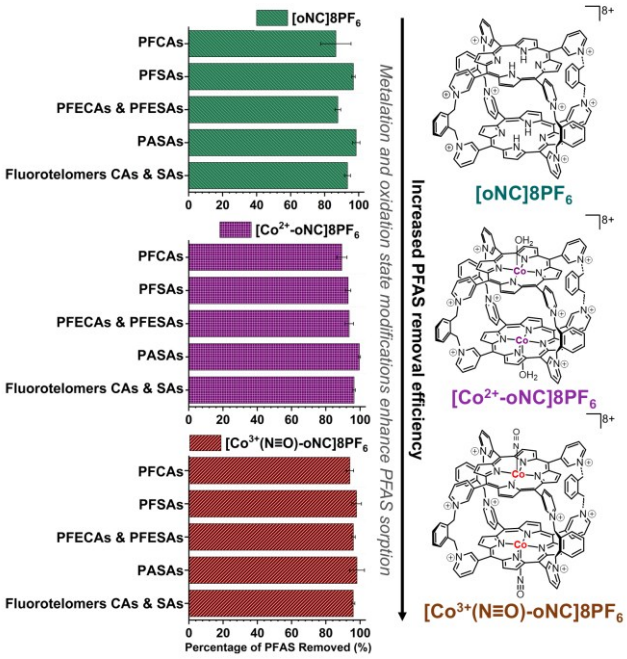

Figure 3. Percent removal efficiencies of porphyrin-based cationic nanocages **[oNC]8PF$_6$** (*top*), **[Co^{2+}-oNC]8PF$_6$** (middle) and **[Co^{3+}(N≡O)-oNC]8PF$_6$** (*bottom*) for 38 PFAS compounds categorized into five groups: PFCAs (perfluoroalkyl carboxylic acids), PFSAs (perfluoroalkyl sulfonic acids), PFECAs & PFESAs (perfluoroalkyl ether carboxylic and sulfonic acids), PASAs (perfluoroalkane sulfonamido substances), and Fluorotelomers CAs & SAs (carboxylic and sulfonic fluorotelomers).

Table 1. Percentage of PFAS removal for compounds with six or fewer carbons in their structure.

No. of Carbons	PFAS Compound	Removal Efficiency for short-carbon chain PFAS (%)[a]		
		[oNC]8PF$_6$	**[Co^{2+}-oNC]8PF$_6$**	**[Co^{3+}(N≡O)-oNC]8PF$_6$**
4	PFBA	67 ± 3	73 ± 4	84 ± 1
	PFMPA	70 ± 5	82 ± 6	89 ± 2
	PFEESA	90 ± 2	97.5 ± 1	98 ± 0.5
	PFBS	95 ± 0.3	96 ± 1	99 ± 1
5	PFPeA	82 ± 3	84 ± 0.5	92 ± 2
	PFMBA	82 ± 4	93 ± 3	92 ± 3
	NFDHA	86 ± 5	97 ± 1	97 ± 1
	PFPeS	94 ± 4	96 ± 1	99 ± 0.5
6	3:3 FTCA	78 ± 2	88 ± 2	83 ± 2
	GenX	90 ± 4	88 ± 7	98 ± 2
	4:2 FTS	92.5 ± 6	98 ± 1	99 ± 1
	PFHxA	94 ± 1	94 ± 1.5	95 ± 1
	PFHxS	98.5 ± 1	99 ± 0.1	99 ± 0.5

[a]Mean PFAS removal percentage calculated from experiment repetitions (n), presented as mean ± SD, where $3 \leq n < 6$.

Although the **[Co^{3+}(N≡O)-oNC]8PF_6** nanocage achieves the highest removal efficiencies, its synthesis involves additional steps, including the chemical oxidation of Co^{2+} with nitric oxide, and presents a lower reaction yield (~56%) compared to the other nanocages (>90%). To reduce materials cost, improve practicality and retain performance, we proposed a mixture of **[oNC]8PF_6** and **[Co^{2+}-oNC]8PF_6**. We tested a range of complementary weight ratios (1:9 to 9:1) while maintaining a total load of 9 mg/mL. As shown in Figure S8, ta 1:4 (**[oNC]8PF_6**:**[Co^{2+}-oNC]8PF_6**) ratio was optimal for PFAS removal, with enhanced efficiency for shorter-chain PFAS (Figure 4A). This effect likely arises from the metalated cages influencing the local environment around non-metalated cages, potentially modifying the ionic strength or pH of the matrix. The combination of non-metalated and cobalt-metalated oNCs provides a wider range of adsorption sites: non-metalated nanocages capture a broader spectrum of molecules, while metalated selectively bind specific PFAS, particularly shorter-chain carboxylic acids. This complementarity improves the overall PFAS removal efficiency.

In the following section, the nanocage mixture was systematically evaluated for its PFAS removal efficiency across various buffered pH aqueous solutions, real-world water matrices (influent sewage and groundwater, see Figure S9), and its potential for recyclability. These assessments revealed optimal performance at neutral pH, with reduced efficiency under acidic and basic conditions. In environmental water matrices, the presence of organic matter and high ionic strength decreased the capture of short-chain PFAS. Additionally, the nanocages exhibited potential for recyclability, maintaining high removal efficiency over three cycles, and demonstrated superior performance compared to activated carbon within a 15-minute contact timeframe.

3.3 Removal at various pH levels

The removal efficiencies of PFAS using the 1:4 (**[oNC]8PF_6**:**[Co^{2+}-oNC]8PF_6**) mixture revealed a significant variance across different pH levels. Specifically, the removal rate was found to be optimal at neutral pH, where the nanocage facilitated the most effective sorption of PFAS from water. Conversely, under more acidic (pH = 3) and basic (pH = 10) conditions, the efficiency significantly decreased. For PFBA, PFPeA, and 3:3 FTCA, the sorption efficiencies dropped from 80-90% at neutral pH to 60% at pH = 3, and similarly for PFBA, PFMPA, and 3:3 FTCA at pH = 10 (Figure S10). Additionally, most PFESAs and PFECAs exhibited reduced removal under these more extreme pH conditions (Figure 4B, Table S5). This variation in performance can be attributed to pH-dependent structural and charge modifications in several PFAS substances, which alter the electrostatic and hydrophobic interactions between the nanocage mixture and PFAS. Furthermore, the presence of other organic buffer molecules in acidic and basic conditions may also impact these interactions. Overall, at neutral pH, the cages remove on average 91-95% of the PFAS in the mixture.

3.4 Influent sewage water and groundwater matrix tests

To explore the efficiency of the nanocage mixture in removing PFAS from real environmental matrices, we investigated influent sewage water and groundwater spiked with 38 different PFAS at a concentration of 50 ng/mL, employing the optimized equilibration time of 15 minutes and loading of 9 mg/mL of cage. In both sewage and groundwater matrices, the capture of most PFAS approached 100% (Figure 4C), particularly for species with sulfonated head groups (Figure S12); however, despite prior optimization of parameters, the capture efficiencies for PFAS with chain lengths shorter than C6 showed notable decline in ground and influent sewage water compared to Nanopure^{TM} water (Figure S12): (*i*) for PFCAs, e.g. PFBA, PFPeA, and PFHxA, efficiency decreased from 80%, 90%, and 95% to approximately 40%, 60%, and 80%, respectively; (*ii*) for fluorotelomers, e.g. 3:3 FTCA and 4:2 FTS, it decreased from 90% and 95% to 40% and 80%, respectively; and (*iii*) for perfluoroether-based substances, e.g. PFMPA, PFMBA, NFDHA, and HFPO-DA, it dropped from an overall 80-95% to 60-65% (See Table S6). The reduced binding efficiencies can be attributed to competition for binding sites from organic matter and ions present in the water, caused by high total organic content (TOC) and ionic strength (conductivity) (see *Supporting Information*). Our group has observed similar effects of increasing ionic strength and natural organic matter on PFOS and PFOA removal by other types of sorbents, such as by graphene and zero-valent-iron based nanohybrids,[78] which reduced binding efficiencies of PFAS. We do not attribute any pH effects to the reduced removal efficiencies since our influent sewage and ground water matrices had an overall neutral pH of 7.4 and 6.9, respectively.[79]

3.5 Recyclability and benchmarking against Activated Carbon

The responsive behavior of molecular nanocages to acidic and basic stimuli, which facilitates the expulsion of encapsulated guests, presents a method for facile regeneration and recyclability.[80, 81] This characteristic could substantially reduce both operational costs and environmental impact. Figure S12 shows the sustained performance of nanocage mixtures over three regeneration cycles, where a methanolic NaCl treatment regenerates the adsorbent by disrupting hydrophobic and electrostatic interactions. Methanol reduces solution polarity and surface tension, weakening PFAS binding, while ionic strength and salting-out effect of NaCl promote PFAS release, restoring the adsorbent capacity.[82] Generally, a modest decline in removal efficiency was observed with each subsequent cycle, which is consistent with the anticipated wear and partial saturation of the nanocage sorption sites. This stability in performance, despite repeated use, highlights the robustness of these nanocages in maintaining efficacy over time. Moreover, to benchmark the nanocages performance, we conducted a comparison analysis against equal loadings of activated carbon (CAS No. 7440-44-0) (See Figure 4D, S13). In 15 minutes, the nanocages achieved ~97% removal of both PFSAs and PASAs, surpassing the 65% and 80% removal rates observed with activated carbon. While both materials were tested for the same duration, activated carbon is known to require longer times to reach adsorption equilibrium, highlighting the superior efficiency of the nanocages in shorter time frames.[82-84]

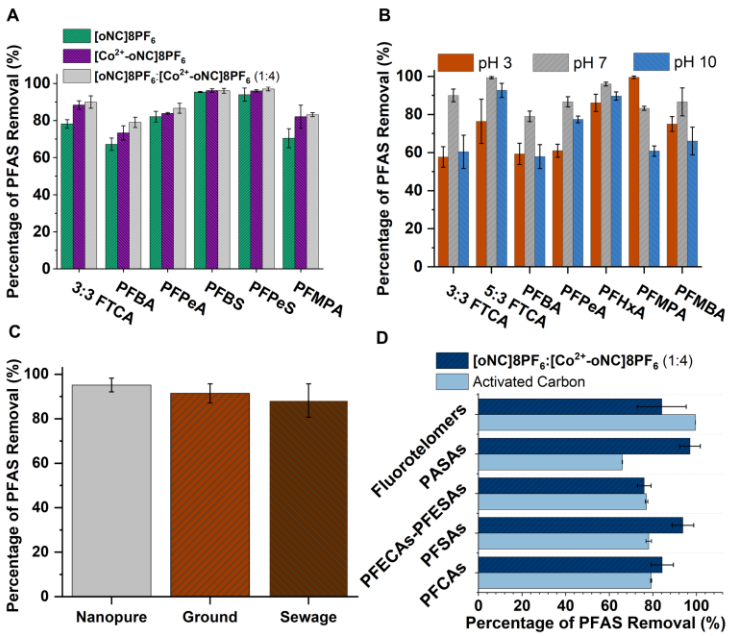

Figure 4. Efficiency of PFAS removal across different conditions by a 1:4 (**[oNC]8PF6**:**[Co2+-oNC]8PF6**) mixture. (**A**) Comparison of removal efficiencies for six representative short-chain PFAS in a spiked Nanopure™ water matrix using pure **[oNC]8PF6** (green), pure **[Co2+-oNC]8PF6** (purple), and a 1:4 mixture of **[oNC]8PF6** to **[Co2+-oNC]8PF6** (gray). (**B**) Efficacy of short-chain PFAS removal at varying pH: 3, 7 and 10. (**C**) Mean removal percentages of 38 PFAS in three water matrices: Nanopure™, ground and influent sewage water. (**D**) Average removal efficiency across the five primary PFAS categories over three usage cycles of the mixture.

3.6 Mechanisms of PFAS adsorption

To investigate the interactions of the nanocages with PFAS, focusing specifically on the sorption mechanism in a homogeneous aqueous system, we synthetically modified nanocage **[oNC]8PF6**, by changing the counterion from PF_6^- to Br^- to render nanocage **[oNC]8Br**. While this water-soluble nanocage can provide significant insights into hydrophilic and surface interactions, it might not fully capture the behavior of PFAS with **[oNC]8PF6** where hydrophobic interactions may dominate; however, these experiments are valuable for understanding the overall nanocage representative behavior. We employed a Job plot analysis of NMR data to quantify the binding nanocage:PFOS and nanocage:PFBA stoichiometries. These titrations showcased subtle shifts in peak positions that correspond to the **a**, **d**, **e** and **g** protons of the soluble cage with varying molar equivalents of PFOS and PFBA, suggesting alterations in the cage lateral local chemical environment (Figure 5A, S15A, respectively). The job plot for PFBA was linear (Figure S15B), this could suggest that the binding is continuous or involves weak, non-specific interactions (like aggregation or very weak binding) between the PFBA and the oNC over the range of concentrations we studied. On the other hand, the experiment with PFOS revealed that a stable complex formation occurred at a 1:8 molar ratio (cage to PFAS). At this specific ratio, we observed

the formation of an insoluble complex, necessitating a shift to deuterated acetonitrile as the solvent for further NMR analysis. Subsequent ^{1}H and ^{19}F NMR studies in this solvent confirmed the successful incorporation of perfluorooctanesulfonic acid (PFOS) into the nanocage structure, suggesting the replacement of eight bromide ions (8Br) with eight PFOS anions that are needed for charge balance (See Figure S15C and S15D). This is an interesting observation because PFAS adsorption mechanisms are known to encompass not only electrostatic and hydrophobic interactions but also anion and ligand exchange processes.[1] We attempted to grow crystals of an anion-exchanged complex, but after several attempts, no crystals suitable for SCXRD were obtained.

To gain a better understanding of the mechanism of PFAS sorption onto the nanocages, we employed density functional theory (DFT) calculations. These computational analyses allowed us to investigate the specific binding interactions between PFAS molecules and the nanocage, revealing preferential binding sites and the strength of these interactions. Across all PFAS molecules analyzed, the binding energy ($\Delta E_{binding}$) was consistently negative, indicating favorable interactions (Figure 5C). Notably, the binding energy increased with the length of the perfluoroalkyl chain. Among the PFAS molecules studied, perfluorobutanesulfonic acid (PFBS) exhibited the lowest binding energy magnitudes, with values of –11.6, –11.0, –9.4, and –8.3 kcal/mol for BP86-D3(BJ), PBE-D3(BJ), PBE0-D3(BJ), and TPSS-D3(BJ) functionals, respectively. Conversely, perfluoroheptanesulfonic acid (PFHpS) and perfluorooctanesulfonic acid (PFOS) demonstrated the highest binding energies, with PFHpS showing –20.1, –15.8, –15.9, and –15.0 kcal/mol, and PFOS showing –17.0, –15.2, –14.0, and –15.7 kcal/mol across these functionals, respectively. These findings align with our experimental observations, which indicate a preference for PFAS molecules with carbon chains of five or more carbons. On the other hand, these results also revealed a strong preference for PFAS to bind within the interior of the nanocage rather than on its exterior (Figure 5D and S14). Ultimately, we attribute the higher binding energy observed for long-chain PFAS to van der Waals forces, electrostatic interactions, and conformational energetics that likely favor the overall stronger binding. However, to fully understand the thermodynamics driving these interactions, further investigations using energy decomposition analysis (EDA) and vibrational frequency calculations from our DFT results are needed. These analyses will help clarify the spontaneity of the adsorption process and the underlying reasons for the differences in binding strength. It is our future goal to highlight the results of these calculations in a future manuscript that is focused on the thermodynamics reasons for the differences in binding, and other bonding decomposition arguments that would result from a fragment orbital calculation. These discussions have been delayed due to the high computational cost of these aforementioned vibrational frequency calculations.

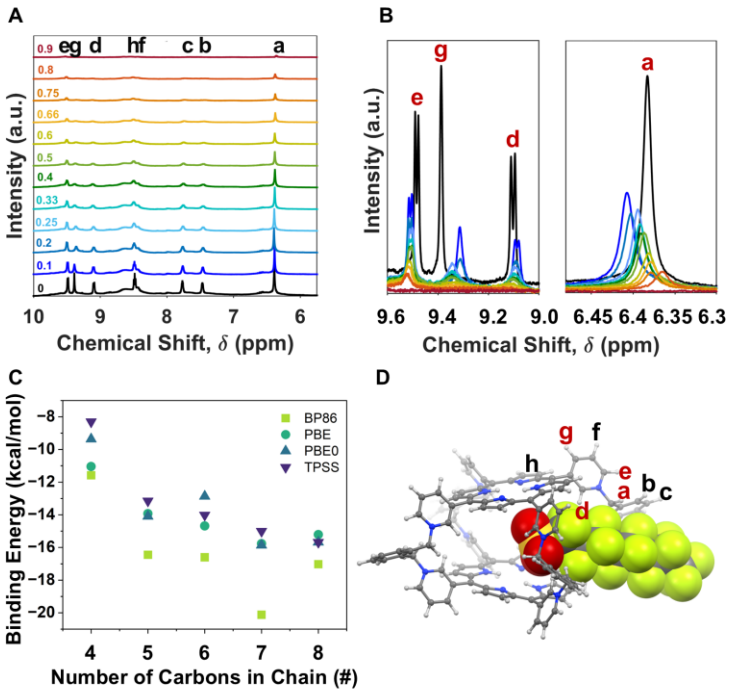

Figure 5. (**A**) ^{1}H-NMR spectra obtained from titrations of 3.0 mM PFOS D_2O solution into 3mM of **[oNC]8Br**, illustrating the subtle shifts over 0 to 0.9 mol fraction (χ_A); (χ_A) = [PFOS]/([PFOS]+[**[oNC]8Br**]). (**B**) Specific ^{1}H-NMR regions where shifts in the peaks are evident, emphasizing the changes in the local proton environments. (**C**) Graphical representation of binding energies for perfluoroalkyl sulfonic acids (PFSAs) ranging from 4 to 8 carbon atoms in their structural chains. (**D**) Optimized 3D geometry of a PFO- molecule interacting with the **[oNC]8PF$_6$** cage.

3.7 Addressing the safety of oNCs through eco-toxicity measurements

This section discusses the methodologies and findings of ecotoxicity assessments conducted on **[oNC]8PF$_6$** and **[Co^{2+}-oNC]8PF$_6$** nanocages, proposing such evaluations as a necessity in the early stages of promising environmental technology development.

3.7.1 Zebrafish Embryo Survival is Unaltered at oNCs Concentrations Below 2.5 μM

Although the nanocages are inherently hydrophobic; they may gradually solvate over time, underscoring the necessity for a threshold assessment to determine the leaching molarity at which significant impacts to fish could occur. Single embryos were placed in 24-well plates with concentrations of 2.5, 0.5, and 0.05 μM, and control egg water, for both **[oNC]8PF$_6$** and **[Co^{2+}-oNC]8PF$_6$** at 24 hours post-fertilization (hpf). Fish were monitored every 12 hours to 11.5 days post-fertilization (dpf) (Figure 6). Lethality was observed only at the 2.5 μM concentration. For **[oNC]8PF$_6$**, 10% lethality occurred after 12 hours, 90% after 24 hours, and complete mortality by 36 hours. **[Co^{2+}-oNC]8PF$_6$** exposure resulted in 10% lethality after 24 hours, 30% after 36 hours, 60% after 48 hours, with complete mortality by 60 hours. These results indicate that zebrafish embryos tolerate both nanocages at concentrations below 2.5 μM.

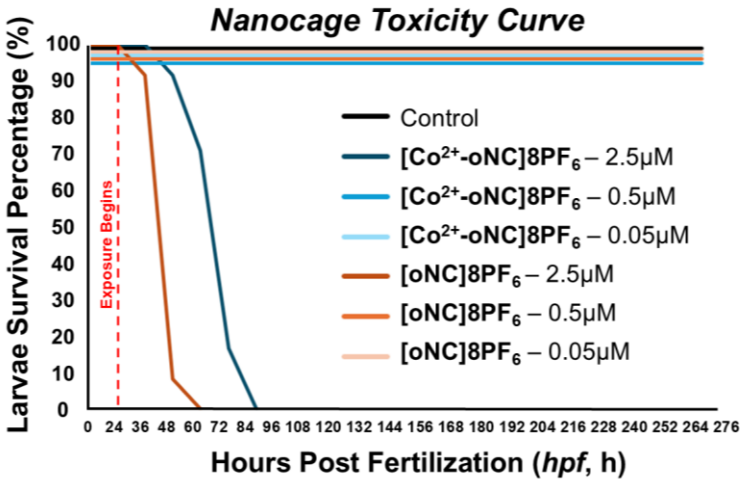

Figure 6. Assessment of the impacts of nanocage compounds on zebrafish. Zebrafish embryos were exposed to **[oNC]8PF$_6$** and **[Co^{2+}-oNC]8PF$_6$** at three concentrations (2.5, 0.5, 0.05 μM) and vehicle control egg water starting at 24 hpf. Lethality was recorded every 12 hours for 11.5 5 days post-fertilization (dpf).

3.7.2 Impacts of oNCs on spontaneous locomotor activity and photic responses in Zebrafish larvae

Although concentrations of both types of nanocage did not produce overt toxicity at concentrations below 2.5 μM, we sought to determine whether lower concentrations of the nanocages might have subtler impacts. We conducted a sensitive photic-evoked locomotion behavioral assay to broadly assess the effect of these compounds on zebrafish larval development. In this assay, locomotor behavior was monitored in the light for 15 minutes, at which time the illumination was extinguished to induce a startle like response, followed by 15 minutes of darkness. Movement distance, count, and duration were recorded for 6-day post-fertilization (dpf) larvae in 24-well plates for both light and dark conditions (See Figure S16). For **[oNC]8PF$_6$** exposure, there was a significant effect for larvae treated with 0.5 μM in both the light and dark conditions. In the light, the 0.5 μM concentration showed increased distance, movement counts, and duration. In contrast, in the dark, larvae treated with this concentration showed hypoactivity. As for the other treatment concentrations, only 0.005 μM showed a significant effect in the light for hypoactive movement count. The photic response was not impacted by any of the treatments. On the other hand, **[Co^{2+}-oNC]8PF$_6$** treatment at 0.05 μM resulted in diminished distance travelled, movement counts, and duration in the light. In addition, increased distance travelled was observed in larvae treated with 0.5 μM. In dark conditions, only 0.05 and 0.5 μM showed diminished distance travelled, movement counts, and duration. As with **[oNC]8PF$_6$**, the photic response was not altered. While additional safety assessments are needed, together these results suggest that concentrations of these nanocages of 0.005 μM and below do not overtly impact zebrafish larval locomotor behavior. Given potential leaching-related risks, despite the material's hydrophobicity, we suggested that the material be used in an immobilized form within a polymer

matrix for long-term applications (mixed-matrix membrane). This approach could prevent leaching and enhance stability and effectiveness, similar to how activated carbon is used in adsorption chambers.

4. Environmental Implication

The utilization of porphyrin-based organic nanocages for PFAS removal represents a promising approach for sustainable water remediation. Although porphyrin-based materials could have a higher initial cost, their exceptional reusability may offset this expense over time. In contrast to the energy-intensive processes needed for activated carbon, they require only mild regeneration, such as ethanolic washing. This lower energy demand could play a role in reducing overall costs and environmental impact. Additionally, their selective adsorption enables more efficient removal of specific contaminants, especially in complex water matrices where targeted pollutant removal is crucial. Our study demonstrated that chemical modifications to the structure of these oNCs, including metalation and metal oxidation, significantly enhance the average removal efficiency for a mixture of 38 PFAS compounds, including GenX, at a concentration of 50 ng/mL. We observed that the adsorption sites for PFAS within the cage are located between the xylene spacers, with binding energies being more favorable for longer chain PFAS compared to shorter chains. Additionally, our studies highlighted the selectivity for PFAS with higher electron density head groups, such as sulfonates and sulfonamides, and for carbon chain lengths of five carbons or more. This selectivity is likely due to the low electron density imparted by the pyridinium moieties and size compatibility. Furthermore, a 1:4 mixture of **[oNC]8PF$_6$** and **[Co^{2+}-oNC]8PF$_6$** demonstrated durability through three methanolic regeneration cycles, maintaining high performance across neutral pH conditions in different water matrices, including groundwater and sewage water. Benchmarking against activated carbon, typically used in water treatment systems, revealed that the nanocages exhibited superior performance in eliminating PSAF and PFSAs types of PFAS after only 15 minutes of equilibration. The toxicology assessment concluded that the current composition of these nanocages, if leached, is safe below 0.005 μM, approximately 100 ng/mL. Future research will explore optimizing the counterion by changing from hexafluorophosphate (PF_6^-) to bicarbonate (HCO_3^-) or fluoride (F^-). Additionally, the central metal ions may be substituted to address environmental injustices tied to raw material sourcing. These optimizations are expected to enhance the efficacy, sustainability and safety of the nanocages. To maintain water insolubility, potential approaches include immobilizing the nanocages in a polymer membrane, thereby enhancing material properties while preserving performance. Integrating porphyrin-based nanocages into existing water treatment methods could advance mitigation efforts for PFAS removal in the environment.

ASSOCIATED CONTENT

Supporting Information

The Supporting Information is available free of charge on the ACS Publications website.

Materials for LC-MS, UV-Vis, SEM, Mass Spectra, Plots and Tables of PFAS Removal, Crystallographic Details, ^{1}H and ^{19}F NMR spectra of 1:8 cage:PFOS complex, Spontaneous, and Light Evoked Locomotor Behavior in Zebrafish Larvae Exposed to Nanocage Compounds. (PDF)

AUTHOR INFORMATION

Corresponding Authors

*E-mail: krs32@buffalo.edu

*E-mail: trcook@buffalo.edu

*E-mail: dianaaga@buffalo.edu

Authors

Daoyang Zhang, Department of Chemistry, University at Buffalo, The State University of New York, Buffalo, New York 14260, United States.

Scott M. Simpson, Department of Chemistry, St. Bonaventure University, St. Bonaventure, New York 14778, United States.

Mindula K. Wijayahena, Department of Chemistry, University at Buffalo, The State University of New York, Buffalo, New York 14260, United States.

Gina Rizzo, Department of Neurobiology and Behavior, Stony Brook University, Stony Brook, New York 11794, United States.

John Michael Aguilar, Department of Chemistry, University at Buffalo, The State University of New York, Buffalo, New York 14260, United States.

Liezel Mari Abaya, Department of Chemistry, University at Buffalo, The State University of New York, Buffalo, New York 14260, United States.

Julia M. Dovi, Department of Neurobiology and Behavior, Stony Brook University, Stony Brook, New York 11794, United States.

Howard I. Sirotkin, Department of Neurobiology and Behavior, Stony Brook University, Stony Brook, New York 11794, United States.

Matthew R. Crawley, Department of Chemistry, University at Buffalo, The State University of New York, Buffalo, New York 14260, United States.

Notes

The authors declare no competing financial interests.

Acknowledgements

This material is based upon work supported by the National Science Foundation MPS-Ascend Postdoctoral Research Fellowship under Grant CHE-2316525 to K.R.S.L. The authors acknowledge NSF Awards CHE-1847950 to T.R.C and CHE-1905274 to D.S.A. S.M.S. acknowledges support from the Camille & Henry Dreyfus Foundation (TH-23-033). We thank Dr. Alan Friedman for HRMS data collection at the University at Buffalo (UB) Science & Engineering Shared Facilities. NMR experiments were conducted at the UB NMR Center using the NEO 500 MHz NMR spectrometer, funded by NSF CHE-2018160. Single-crystal X-ray diffraction was performed at the UB diffraction facility using the Rigaku XtaLAB Synergy-S, funded by NSF CHE-2216151. We thank E.S. for his assistance with sample preparation and mass measurements. We also thank M.A.A. for assistance with TOC measurements. Any opinions, findings, conclusions, or recommendations expressed in this publication are those of the authors and do not necessarily reflect the view of the NSF.

References

(1) Lei, X.; Lian, Q.; Zhang, X.; Karsili, T. K.; Holmes, W.; Chen, Y.; Zappi, M. E.; Gang, D. D. A Review of PFAS Adsorption from Aqueous Solutions: Current Approaches, Engineering Applications, Challenges, and Opportunities. *Environ. Pollut.* **2023**, *321*, 121138.
(2) Sharma, N.; Kumar, V.; Sugumar, V.; Umesh, M.; Sondhi, S.; Chakraborty, P.; Kaur, K.; Thomas, J.; Kamaraj, C.; Maitra, S. S. A comprehensive review on the need for integrated strategies and process modifications for per- and polyfluoroalkyl substances (PFAS) removal: Current insights and future prospects. *Case Stud. Chem. Environ. Eng* **2024**, *9*, 100623.
(3) Liu, F.; Pignatello, J. J.; Sun, R.; Guan, X.; Xiao, F. A Comprehensive Review of Novel Adsorbents for Per- and Polyfluoroalkyl Substances in Water. *ACS ES&T Water* **2024**, *4* (4), 1191-1205.
(4) Rojas, S.; Horcajada, P. Metal–Organic Frameworks for the Removal of Emerging Organic Contaminants in Water. *Chem. Rev.* **2020**, *120* (16), 8378-8415.
(5) Zhou, J.; Song, M.; Hu, X.; Zhang, W.-x.; Deng, Z. Environmental applications of nanocellulose scaffolded metal organic frameworks (MOFs@NC). *Crit. Rev. Environ. Sci. Technol.* **2023**, *53* (17), 1586-1612.
(6) Sun, Y.; Zhang, N.; Yue, Y.; Xiao, J.; Huang, X.; Ishag, A. Recent advances in the application of zeolitic imidazolate frameworks (ZIFs) in environmental remediation: a review. *Environ. Sci. Nano* **2022**, *9* (11), 4069-4092.
(7) Aslam, A. A.; Irshad, A.; Nazir, M. S.; Atif, M. A review on covalent organic frameworks as adsorbents for organic pollutants. *J. Clean. Prod.* **2023**, *400*, 136737.
(8) Zadehnazari, A.; Khosropour, A.; Zarei, A.; Khazdooz, L.; Amirjalayer, S.; Auras, F.; Abbaspourrad, A. Viologen-Derived Covalent Organic Frameworks: Advancing PFAS Removal Technology with High Adsorption Capacity. *Small* **2024**, 2405176.

(9) Liu, X.; Liu, G.; Fu, T.; Ding, K.; Guo, J.; Wang, Z.; Xia, W.; Shangguan, H. Structural Design and Energy and Environmental Applications of Hydrogen-Bonded Organic Frameworks: A Systematic Review. *Adv. Sci.* **2024**, *11* (22), 2400101.
(10) Zhang, Y.; Tian, M.; Majeed, Z.; Xie, Y.; Zheng, K.; Luo, Z.; Li, C.; Zhao, C. Application of Hydrogen-Bonded Organic Frameworks in Environmental Remediation: Recent Advances and Future Trends. *Separations* **2023**, *10* (3), 196.
(11) Percástegui, E. G. Metal–organic cages against toxic chemicals and pollutants. *Chem. Commun.* **2022**, *58* (33), 5055-5071.
(12) He, Y.; Zhou, J.; Li, Y.; Yang, Y.-D.; Sessler, J. L.; Chi, X. Fluorinated Nonporous Adaptive Cages for the Efficient Removal of Perfluorooctanoic Acid from Aqueous Source Phases. *J. Am. Chem. Soc.* **2024**, *146* (9), 6225-6230.
(13) Das Bairagya, M.; Ntipouna, P. S.; Stewart, N. K.; Elgrishi, N. A molecular metal–organic cage as a recyclable sponge for PFOS removal from water. *Chem. Commun.* **2024**, *60* (79), 11084-11087.
(14) Takezawa, H.; Murase, T.; Resnati, G.; Metrangolo, P.; Fujita, M. Recognition of Polyfluorinated Compounds Through Self-Aggregation in a Cavity. *J. Am. Chem. Soc.* **2014**, *136* (5), 1786-1788.
(15) Fulong, C. R. P.; Guardian, M. G. E.; Aga, D. S.; Cook, T. R. A Self-Assembled Iron(II) Metallacage as a Trap for Per- and Polyfluoroalkyl Substances in Water. *Inorg. Chem.* **2020**, *59* (10), 6697-6708.
(16) Camdzic, D.; Welgama, H. K.; Crawley, M. R.; Avasthi, A.; Cook, T. R.; Aga, D. S. Rapid Capture of Per- and Polyfluoroalkyl Substances Using a Self-Assembling Zirconium-Based Metal-Organic Cage. *ACS Appl. Energy Mater.* **2024**, *2* (1), 87-95.
(17) Mollick, S.; Fajal, S.; Mukherjee, S.; Ghosh, S. K. Stabilizing Metal–Organic Polyhedra (MOP): Issues and Strategies. *Chem. Asian J.* **2019**, *14* (18), 3096-3108.
(18) Wang, H.; Jin, Y.; Sun, N.; Zhang, W.; Jiang, J. Post-synthetic modification of porous organic cages. *Chem. Soc. Rev.* **2021**, *50* (16), 8874-8886.
(19) Segura, J. L.; Royuela, S.; Mar Ramos, M. Post-synthetic modification of covalent organic frameworks. *Chem. Soc. Rev.* **2019**, *48* (14), 3903-3945.
(20) Martín Díaz, A. E.; Lewis, J. E. M. Structural Flexibility in Metal-Organic Cages. *Front. Chem.* **2021**, *9*.
(21) La, D. D.; Dang, T. D.; Le, P. C.; Bui, X. T.; Chang, S. W.; Chung, W. J.; Kim, S. C.; Nguyen, D. D. Self-assembly of monomeric porphyrin molecules into nanostructures: Self-assembly pathways and applications for sensing and environmental treatment. *Environ. Technol. Innov.* **2023**, *29*, 103019.
(22) Wang, Y.; Cui, X.; Zhang, P.; Wang, Y.; Lu, W. Synthesis of porphyrin porous organic polymers and their application of water pollution treatment: A review. *Environ. Technol. Innov.* **2023**, *29*, 102972.
(23) Zhao, S.; Li, S.; Zhao, Z.; Su, Y.; Long, Y.; Zheng, Z.; Cui, D.; Liu, Y.; Wang, C.; Zhang, X.; Zhang, Z. Microwave-assisted hydrothermal assembly of 2D copper-porphyrin metal-organic frameworks for the removal of dyes and antibiotics from water. *Environ. Sci. Pollut. Res. Int.* **2020**, *27* (31), 39186-39197.
(24) Lee, M. Y.; Ahmed, I.; Yu, K.; Lee, C.-S.; Kang, K.-K.; Jang, M.-S.; Ahn, W.-S. Aqueous adsorption of bisphenol A over a porphyrinic porous organic polymer. *Chemosphere* **2021**, *265*, 129161.

(25) Wang, J.; Jiao, C.; Li, M.; Wang, X.; Wang, C.; Wu, Q.; Wang, Z. Porphyrin based porous organic polymer modified with Fe3O4 nanoparticles as an efficient adsorbent for the enrichment of benzoylurea insecticides. *Mikrochim. Acta* **2017**, *185* (1), 36.
(26) Li, Z.-J.; Xue, H.-D.; Zhang, Y.-Q.; Hu, H.-S.; Zheng, X.-D. Construction of a cationic organic network for highly efficient removal of anionic contaminants from water. *New J. Chem.* **2019**, *43* (29), 11604-11609.
(27) Sun, J.; Jennepalli, S.; Lee, M.; Jones, A.; O'Carroll, D. M.; Manefield, M. J.; Bhadbhade, M.; Åkermark, B.; Das, B.; Kumar, N. Efficient Reductive Defluorination of Branched PFOS by Metal–Porphyrin Complexes. *Environ. Sci. Technol.* **2022**, *56* (12), 7830-7839.
(28) Zhu, Z.-H.; Liu, Y.; Song, C.; Hu, Y.; Feng, G.; Tang, B. Z. Porphyrin-Based Two-Dimensional Layered Metal–Organic Framework with Sono-/Photocatalytic Activity for Water Decontamination. *ACS Nano* **2022**, *16* (1), 1346-1357.
(29) Zhang, Y.; Kong, K.; Wu, Q.; Ma, T.; Liang, J.; Wang, R. A Porphyrinic Metal-Organic Framework with Cooperative Adsorption Domains for PFAS Removal from Water. *ChemSusChem* **2024**, *17* (9), e202400069.
(30) U.S. Environmental Protection Agency. *Draft Method 1633 Analysis of Per- and Polyfluoroalkyl Substances (PFAS) in Aqueous, Solid, Biosolids, and Tissue Samples by LC-MS/MS*. https://www.epa.gov/system/files/documents/2021-09/method_1633_draft_aug-2021.pdf (accessed August 2021).
(31) U.S. Environmental Protection Agency. *Human Health Toxicity Assessments for GenX Chemicals*. https://www.epa.gov/chemical-research/human-health-toxicity-assessments-genx-chemicals (accessed March 2024).
(32) Zhang, D.; Snider, R. L.; Crawley, M. R.; Fang, M.; Sanchez-Lievanos, K. R.; Ang, S.; Cook, T. R. Gram-Scale, One-Pot Synthesis of a Cofacial Porphyrin Bridged by Ortho-xylene as a Scaffold for Dinuclear Architectures. *Inorg. Chem.* **2024**.
(33) Chen, H.; Roy, I.; Myong, M. S.; Seale, J. S. W.; Cai, K.; Jiao, Y.; Liu, W.; Song, B.; Zhang, L.; Zhao, X.; et al. Triplet–Triplet Annihilation Upconversion in a Porphyrinic Molecular Container. *J. Am. Chem. Soc.* **2023**, *145* (18), 10061-10070.
(34) Blackburn, P. T.; Mansoor, I. F.; Dutton, K. G.; Tyryshkin, A. M.; Lipke, M. C. Accessing three oxidation states of cobalt in M6L3 nanoprisms with cobalt–porphyrin walls. *Chem. Commun.* **2021**, *57* (86), 11342-11345.
(35) Labanowski, J. K.; Andzelm, J. W. *Density Functional Methods in Chemistry*; Springer New York, 2012.
(36) Hanwell, M. D.; Curtis, D. E.; Lonie, D. C.; Vandermeersch, T.; Zurek, E.; Hutchison, G. R. Avogadro: an advanced semantic chemical editor, visualization, and analysis platform. *J. Cheminform.* **2012**, *4* (1), 17.
(37) Balasubramani, S. G.; Chen, G. P.; Coriani, S.; Diedenhofen, M.; Frank, M. S.; Franzke, Y. J.; Furche, F.; Grotjahn, R.; Harding, M. E.; Hättig, C.; et al. TURBOMOLE: Modular program suite for ab initio quantum-chemical and condensed-matter simulations. *J. Chem. Phys.* **2020**, *152*, 184107.
(38) *TURBOMOLE Computer Program v7.3*; (accessed 2023).
(39) Schäfer, A.; Huber, C.; Ahlrichs, R. Fully optimized contracted Gaussian basis sets of triple zeta valence quality for atoms Li to Kr. *J. Chem. Phys.* **1994**, *100* (8), 5829-5835.
(40) Weigend, F.; Häser, M.; Patzelt, H.; Ahlrichs, R. RI-MP2: optimized auxiliary basis sets and demonstration of efficiency. *Chem. Phys. Lett.* **1998**, *294* (1), 143-152.

(41) Vosko, S. H.; Wilk, L.; Nusair, M. Accurate spin-dependent electron liquid correlation energies for local spin density calculations: a critical analysis. *Can. J. Phys.* **1980**, *58* (8), 1200-1211.
(42) Becke, A. D. Density-functional exchange-energy approximation with correct asymptotic behavior. *Phys. Rev. A* **1988**, *38* (6), 3098-3100.
(43) Perdew, J. P.; Ernzerhof, M.; Burke, K. Rationale for mixing exact exchange with density functional approximations. *J. Chem. Phys.* **1996**, *105* (22), 9982-9985.
(44) Perdew, J. P.; Wang, Y. Accurate and simple analytic representation of the electron-gas correlation energy. *Phys. Rev. B* **1992**, *45* (23), 13244-13249.
(45) Perdew, J. P.; Burke, K.; Ernzerhof, M. Generalized Gradient Approximation Made Simple [Phys. Rev. Lett. 77, 3865 (1996)]. *Phys. Rev. Lett.* **1997**, *78* (7), 1396-1396.
(46) Tao, J.; Perdew, J. P.; Staroverov, V. N.; Scuseria, G. E. Climbing the Density Functional Ladder: Nonempirical Meta--Generalized Gradient Approximation Designed for Molecules and Solids. *Phys. Rev. Lett.* **2003**, *91* (14), 146401.
(47) Dirac, P. A. M.; Fowler, R. H. Quantum mechanics of many-electron systems. *Proc. R. soc. Lond. Ser. A-Contain. Pap. Math. Phys. Character* **1929**, *123* (792), 714-733.
(48) Slater, J. C. A Simplification of the Hartree-Fock Method. *Phys. Rev.* **1951**, *81* (3), 385-390.
(49) Grimme, S.; Ehrlich, S.; Goerigk, L. Effect of the damping function in dispersion corrected density functional theory. *J. Comput. Chem.* **2011**, *32* (7), 1456-1465.
(50) Grimme, S.; Antony, J.; Ehrlich, S.; Krieg, H. A consistent and accurate ab initio parametrization of density functional dispersion correction (DFT-D) for the 94 elements H-Pu. *J. Chem. Phys.* **2010**, *132* (15).
(51) Antle, J. P.; LaRock, M. A.; Falls, Z.; Ng, C.; Atilla-Gokcumen, G. E.; Aga, D. S.; Simpson, S. M. Building Chemical Intuition about Physicochemical Properties of C8-Per-/Polyfluoroalkyl Carboxylic Acids through Computational Means. *ACS ES&T Engineering* **2024**, *4* (1), 196-208.
(52) Goss, K.-U. The pKa Values of PFOA and Other Highly Fluorinated Carboxylic Acids. *Environ. Sci. Technol.* **2008**, *42* (2), 456-458.
(53) Lampic, A.; Parnis, J. M. Property Estimation of Per- and Polyfluoroalkyl Substances: A Comparative Assessment of Estimation Methods. *Environ. Toxicol. Chem.* **2020**, *39* (4), 775-786.
(54) Klamt, A.; Schüürmann, G. COSMO: a new approach to dielectric screening in solvents with explicit expressions for the screening energy and its gradient. *J. Chem. Soc., Perkin Trans.* **1993**, (5), 799-805.
(55) Klamt, A. The COSMO and COSMO-RS solvation models. *Wiley Interdiscip. Rev. Comput. Mol. Sci.* **2011**, *1* (5), 699-709.
(56) Endo, S.; Hammer, J.; Matsuzawa, S. Experimental Determination of Air/Water Partition Coefficients for 21 Per- and Polyfluoroalkyl Substances Reveals Variable Performance of Property Prediction Models. *Environ. Sci. Technol.* **2023**, *57* (22), 8406-8413.
(57) Wang, Z.; MacLeod, M.; Cousins, I. T.; Scheringer, M.; Hungerbühler, K. Using COSMOtherm to predict physicochemical properties of poly- and perfluorinated alkyl substances (PFASs). *Environ. Chem.* **2011**, *8* (4), 389-398.
(58) Zhang, M.; Suuberg, E. M. Estimation of vapor pressures of perfluoroalkyl substances (PFAS) using COSMOtherm. *J. Hazard. Mater.* **2023**, *443*, 130185.
(59) Hill, A. J.; Teraoka, H.; Heideman, W.; Peterson, R. E. Zebrafish as a Model Vertebrate for Investigating Chemical Toxicity. *Toxicol. Sci.* **2005**, *86* (1), 6-19.

(60) Huang, I. J.; Sirotkin, H. I.; McElroy, A. E. Varying the exposure period and duration of neuroactive pharmaceuticals and their metabolites modulates effects on the visual motor response in zebrafish (Danio rerio) larvae. *Neurotoxicol. Teratol.* **2019**, *72*, 39-48.
(61) Burgess, H. A.; Granato, M. Modulation of locomotor activity in larval zebrafish during light adaptation. *J. Exp. Biol.* **2007**, *210* (14), 2526-2539.
(62) Emran, F.; Rihel, J.; Dowling, J. E. A behavioral assay to measure responsiveness of zebrafish to changes in light intensities. *J Vis Exp* **2008**, 20, 923.
(63) Kocher, L.; Durot, S.; Heitz, V. Control of the cavity size of flexible covalent cages by silver coordination to the peripheral binding sites. *Chem. Commun.* **2015**, *51* (67), 13181-13184.
(64) García-Simón, C.; Garcia-Borràs, M.; Gómez, L.; Parella, T.; Osuna, S.; Juanhuix, J.; Imaz, I.; Maspoch, D.; Costas, M.; Ribas, X. Sponge-like molecular cage for purification of fullerenes. *Nat. Commun.* **2014**, *5* (1), 5557.
(65) Stulz, E.; Scott, S. M.; Bond, A. D.; Teat, S. J.; Sanders, J. K. M. Selection and Amplification of Mixed-Metal Porphyrin Cages from Dynamic Combinatorial Libraries. *Chem. Eur. J.* **2003**, *9* (24), 6039-6048.
(66) Jökel, J.; Schwer, F.; von Delius, M.; Apfel, U.-P. A dinuclear porphyrin-macrocycle as efficient catalyst for the hydrogen evolution reaction. *Chem. Commun.* **2020**, *56* (91), 14179-14182.
(67) Rothschild, D. A.; Kopcha, W. P.; Tran, A.; Zhang, J.; Lipke, M. C. Gram-scale synthesis of a covalent nanocage that preserves the redox properties of encapsulated fullerenes. *Chem. Sci.* **2022**, *13* (18), 5325-5332.
(68) Crawley, M. R.; Zhang, D.; Oldacre, A. N.; Beavers, C. M.; Friedman, A. E.; Cook, T. R. Tuning the Reactivity of Cofacial Porphyrin Prisms for Oxygen Reduction Using Modular Building Blocks. *J. Am. Chem. Soc.* **2021**, *143* (2), 1098-1106.
(69) Faust, S. D.; Aly, O. M. *Adsorption Processes for Water Treatment*; Elsevier Science, 2013.
(70) Naushad, M.; Lichtfouse, E. *Green Materials for Wastewater Treatment*; Springer International Publishing, 2019.
(71) Koval, A. M.; Jenness, G. R.; Shukla, M. K. Structural investigation of the complexation between vitamin B12 and per- and polyfluoroalkyl substances: Insights into degradation using density functional theory. *Chemosphere* **2024**, *364*, 143213.
(72) Li, S.; Ma, J.; Cheng, J.; Wu, G.; Wang, S.; Huang, C.; Li, J.; Chen, L. Metal–Organic Framework-Based Composites for the Adsorption Removal of Per- and Polyfluoroalkyl Substances from Water. *Langmuir* **2024**, *40* (6), 2815-2829.
(73) Li, D.; Londhe, K.; Chi, K.; Lee, C.-S.; Venkatesan, A. K.; Hsiao, B. S. Functionalized bio-adsorbents for removal of perfluoroalkyl substances: A perspective. *AWWA Water Science* **2021**, *3* (6), e1258.
(74) Tie, L.; Zhang, W.-x.; Deng, Z. Ferrous ion-induced cellulose nanocrystals/alginate bio-based hydrogel for high efficiency tetracycline removal. *Sep. Purif. Technol.* **2024**, *328*, 125024.
(75) Gomri, C.; Benkhaled, B. T.; Cretin, M.; Semsarilar, M. Adsorbent Material Used for the Treatment of Per- and Poly-Fluoroalkyl Substances (PFAS): A Short Review. *Macromol. Chem. Phys.* **2024**, *225* (11), 2400012.
(76) Marciesky, M.; Aga, D. S.; Bradley, I. M.; Aich, N.; Ng, C. Mechanisms and Opportunities for Rational In Silico Design of Enzymes to Degrade Per- and Polyfluoroalkyl Substances (PFAS). *J. Chem. Inf. Model.* **2023**, *63* (23), 7299-7319.
(77) Barpaga, D.; Zheng, J.; Han, K. S.; Soltis, J. A.; Shutthanandan, V.; Basuray, S.; McGrail, B. P.; Chatterjee, S.; Motkuri, R. K. Probing the Sorption of Perfluorooctanesulfonate Using

Mesoporous Metal–Organic Frameworks from Aqueous Solutions. *Inorg. Chem.* **2019**, *58* (13), 8339-8346.
(78) Ali, M. A.; Thapa, U.; Antle, J.; Tanim, E. U. H.; Aguilar, J. M.; Bradley, I. M.; Aga, D. S.; Aich, N. Influence of water chemistry and operating parameters on PFOS/PFOA removal using rGO-nZVI nanohybrid. *J. Hazard. Mater.* **2024**, *469*, 133912.
(79) Gagliano, E.; Sgroi, M.; Falciglia, P. P.; Vagliasindi, F. G. A.; Roccaro, P. Removal of poly- and perfluoroalkyl substances (PFAS) from water by adsorption: Role of PFAS chain length, effect of organic matter and challenges in adsorbent regeneration. *Water Res.* **2020**, *171*, 115381.
(80) Dutton, K. G.; Jones, T. J.; Emge, T. J.; Lipke, M. C. Cage Match: Comparing the Anion Binding Ability of Isostructural Versus Isofunctional Pairs of Metal-Organic Nanocages. *Chem. Eur. J.* **2024**, *30* (2), e202303013.
(81) Zhiquan, L.; Xie, H.; Border, S. E.; Gallucci, J.; Pavlović, R. Z.; Badjić, J. D. A Stimuli-Responsive Molecular Capsule with Switchable Dynamics, Chirality, and Encapsulation Characteristics. *J. Am. Chem. Soc.* **2018**, *140* (35), 11091-11100.
(82) Riegel, M.; Haist-Gulde, B.; Sacher, F. Sorptive removal of short-chain perfluoroalkyl substances (PFAS) during drinking water treatment using activated carbon and anion exchanger. *Environ. Sci. Eur.* **2023**, *35* (1), 12.
(83) Xiao, X.; Ulrich, B. A.; Chen, B.; Higgins, C. P. Sorption of Poly- and Perfluoroalkyl Substances (PFASs) Relevant to Aqueous Film-Forming Foam (AFFF)-Impacted Groundwater by Biochars and Activated Carbon. *Environ. Sci. Technol.* **2017**, *51* (11), 6342-6351.
(84) Gundogdu, A.; Duran, C.; Senturk, H. B.; Soylak, M.; Ozdes, D.; Serencam, H.; Imamoglu, M. Adsorption of Phenol from Aqueous Solution on a Low-Cost Activated Carbon Produced from Tea Industry Waste: Equilibrium, Kinetic, and Thermodynamic Study. *J. Chem. Eng. Data* **2012**, *57* (10), 2733-2743.

TOC

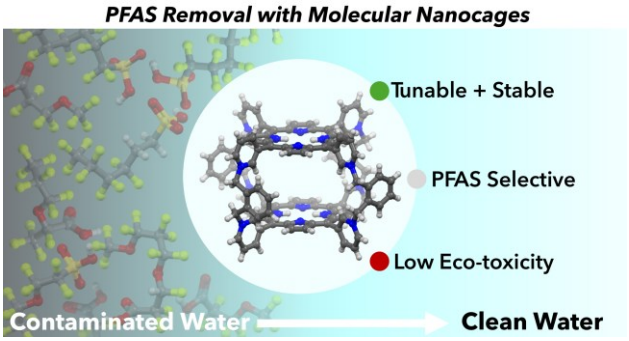
PFAS Removal with Molecular Nanocages
Tunable + Stable
PFAS Selective
Low Eco-toxicity
Contaminated Water
Clean Water